2019

# Numerical Study on the Dynamic Process of Single Plume Flow in Thermal Convection with Polymers

Jian-Ping Cheng

Wei-Hua Cai

Hong-Na Zhang

Feng-Chen Li

Lian Shen

*See next page for additional authors*

Repository Citation

Original Publication Citation

**Authors**

Jian-Ping Cheng, Wei-Hua Cai, Hong-Na Zhang, Feng-Chen Li, Lian Shen, and Shi-Zhi Qian

# Numerical study on the dynamic process of single plume flow in thermal convection with polymers

View Online    Export Citation    CrossMark

Jian-Ping Cheng (程建平),[1,2] [ID] Wei-Hua Cai (蔡伟华),[1,a)] [ID] Hong-Na Zhang (张红娜),[3,a)] [ID] Feng-Chen Li (李凤臣),[3]
Lian Shen (沈炼),[2] and Shi-Zhi Qian (钱诗智)[4]

## AFFILIATIONS

[1] School of Energy Science and Engineering, Harbin Institute of Technology, Harbin 150001, China
[2] Department of Mechanical Engineering, University of Minnesota, Minneapolis, Minnesota 55455, USA
[3] Sino-French Institute of Nuclear Engineering and Technology, Sun Yat-Sen University, Zhuhai 519082, China
[4] Institute of Micro/Nanotechnology, Old Dominion University, Norfolk, Virginia 23529, USA

**Note:** This paper is part of the special issue from the 10th National Congress on Fluid Mechanics of China.
[a)] Authors to whom correspondence should be addressed: caiwh@hit.edu.cn and zhanghn26@mail.sysu.edu.cn

## ABSTRACT

A direct numerical simulation of single plume flow in thermal convection with polymers was carried out in a domain with 1:3 as the width to height ratio. The heat transport ability is weakened by adding polymers within the here-investigated governing parameter range. However, it is promoted when the maximum polymer extension $L$ is increased. The distribution of vertical velocity and temperature indicates that the plume in the polymer solution case is speeded up and widens bigger as compared to that in the Newtonian fluid case. Inside the plume, polymer chains tend to release energy at the position where the velocity is decelerated. The ratio of Nusselt numbers ($Nu/Nu_{New}$) shows the power-law scaling relation with the governing parameter $L^2/Wi$ in polymer solution cases, which is only applicable for moderate $Wi$ and small $L$. The present study can give direct insight into the observation about plumes in turbulent thermal convection experiments. It is therefore useful for the analysis of heat transport in thermal convection with polymers.

Published under license by AIP Publishing. https://doi.org/10.1063/1.5083195

## I. INTRODUCTION

Heat is transported by convection in many natural systems, such as the atmosphere, the magmas, and the Earth's mantle. One of the classical systems to model various convection phenomena is Rayleigh-Bénard convection (RBC), which describes a cell filled with fluid heated from the bottom and cooled on the top.[1,2] Thermal plumes, the most important flow structures in this system, are emitted intermittently from the boundary layer through buoyancy force due to density difference. They cluster together continually, thereby leading to the formation of large-scale circulation and transferring heat across the convection cell.[3,4] They are known to be main heat carriers in turbulent RBC.[5,6] In recent years,

thermal plumes with the presence of polymers have attracted much attention due to the complex interaction between the two.

In a direct numerical simulation (DNS) study, Dubief[7] adopted a finitely extensible nonlinear elastic-Peterlin (FENE-P) model[8] to investigate how the maximum polymer extension $L$ affects plumes and heat transport in RBC with two infinite horizontal and isothermal walls. The difference between heat transport enhancement (HTE) flow and heat transfer reduction (HTR) flow was attributed to the role change of plume elastic energy. The drastic drop of velocity gradient inside the plume causes the relaxation of stretched polymers as they travel in the plume. With the increasing $L$, plumes are not able to sustain more energy contributions. In turbulent bulk flows

of Rayleigh-Taylor convection,[9] the interaction was investigated by adopting the Oldroyd-B viscoelastic model (i.e., the limit of the FENE-P model under the infinite polymer length). However, it was observed that thermal plumes were speeded up and widened, which in turn contributed to a significant HTE. In sum, the polymer effect on energy transfer in thermal plumes is not universal.

In addition to numerical results, a series of experimental studies were also carried out on RBC in the presence of polymers, focusing on the effect of polymer concentration on heat transport and plume coherence. HTR was observed in an experimental investigation on RBC with polymers.[10] Ahlers and Nikolaenko[10] inferred that polymers reduce the temperature perturbations acting upon the boundary layers (BLs) and thereby reduce plume emission which is exceptionally sensitive to polymer concentration. Wei et al.[11] confirmed the above idea based on the reduction of temperature fluctuations in both BL-dominated and bulk-dominated flows, where HTR and HTE effects were exhibited, respectively. Moreover, Wei et al.[12] observed that the generation of plumes is delayed and inhibited and the size of plumes becomes larger in polymer solution cases. It can be explained from the thickening of thermal and viscous BLs based on particle image velocimetry (PIV) results.[13] Further research from Xie et al.[14] concluded that thermal plumes are emitted less and supply less energy to turbulence, but they are more coherent and energetic, and are able to transport heat more efficiently than those in the Newtonian fluid case.

Although the aforementioned studies have provided us with some fundamental understanding about thermal plumes in RBC with polymers, intuitive cognition on single plume flow in the polymer solution case still needs to be directly investigated to support these scenarios. The corresponding results can also contribute to a fundamental understanding for viscoelastic Marangoni-Bénard convection[15] and vapor plumes.[16]

For the Newtonian fluid case, the studies on single plume flow are extensive and historical. During the last few decades, numerical simulations[17–21] and experimental studies[22–25] have investigated the single plume dynamics for a wide range of Rayleigh number and Prandtl number. It has been proved that steady laminar flow of a single plume can actually be well described by the similarity solutions of pertinent boundary-layer equations. Corresponding theories have also been well established recently for the scaling of plume ascent velocity,[26] plume stem structure,[27] and plume growth by entrainment of ambient fluid.[28] However, the occurrence and characteristics of single plume flow in polymer solution cases are still poorly documented and understood. Vajipeyajula et al.[29] numerically investigated the dynamics of single plume flow in FENE-P fluid. However, the results only explained the HTR phenomenon as induced by elasticity and the effect of L was not investigated. Besides, there is still an open research field in terms of what exactly happens inside the plume and the flow at different developing stages in the presence of polymers. The curiosity on the dynamics, morphology, and heat transport of the plume motivates us to investigate single plume flow in thermal convection with polymers.

The rest paper is organized as follows: Section II describes numerical procedures including the mathematical description, boundary conditions, and numerical schemes. The kinetic energy budget equation is also introduced for convenience of mechanism explanation. Section III presents the results about the effect of elasticity and maximum extension length L on heat transport, flow dynamics, and morphology. Finally, the mechanism of energy exchange when polymers travel in the plume is summarized and the conclusions are drawn in Sec. IV.

## II. NUMERICAL PROCEDURE

### A. Computational model and boundary conditions

When heat is released from a small area at the base of a fluid layer, convection develops in an isolated rising element. As long as supplying continuous heat and remaining connected to the source at all time, the single plume can be generated by instabilities in a container with a point heat source. The schematic of setup for generating the single plume is illustrated in Fig. 1, which can be analogous to a line plume in three-dimensional thermal convection experiments.[30] The origin of the Cartesian coordinate system is allocated at the center of the heat source. DNS is performed in the two-dimensional domain with 1:3 as the width (W) to height (H) ratio. The gravity g acts in parallel with the y direction, as shown in Fig. 1. Adiabatic and non-slip boundary conditions are imposed at the top and bottom plates, whereas the fixed-temperature $T_h$ and non-slip boundary condition are used at the heat source. The boundaries in horizontal directions are
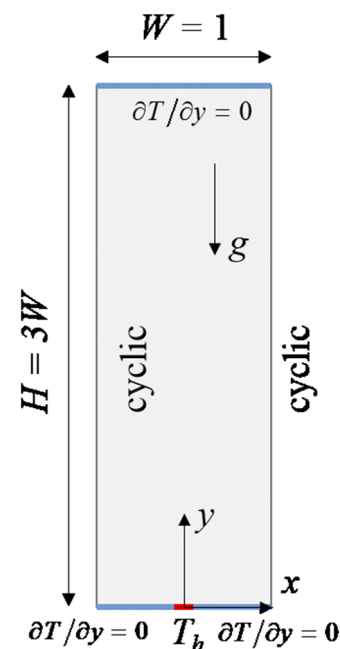


**FIG. 1**. Schematic of the computational model. The dimensionless width of the heat source is $d = 0.01 \times W$.

periodic. The initial temperature and velocity in the internal field are set as zero.

## B. Governing equations

For the flow with polymers, an additional term of elastic stress is added to the Navier-Stokes equations so as to represent the polymer effect. Several types of constitutive models have been developed to describe the polymer effect, such as the Oldroyd-B, FENE-P, and Giesekus models, which have been widely adopted in numerical simulations for turbulent drag-reducing channel flows.[31–33] The FENE-P model,[8] which is based on a dumbbell description of a polymer chain of two equal masses connected by a finitely extensible and nonlinear entropic spring, is utilized to study the nonlinear elastic effect in the present study.

The dimensionless equations are solved in order to make simulation results more universal. The specific dimensionless formulas are defined as follows (here the characteristic scale $H/3$ is used in this paper):

$$x^* = 3x/H, t^* = 3tu_c/H, u_i^* = u_i/u_c, p^* = p/\rho u_c^2, \theta^* = T/T_h,$$

where $(\cdots)^*$ represents the dimensionless parameter; the components of velocity vector $u_i$ are normalized by the characteristic convection velocity $u_c = \sqrt{\alpha g H T_h/3}$; $\alpha$ is the volume expansion coefficient. $T_h$ is the temperature of the heat source; $p$ is the pressure; $\rho$ is the density; $C_{ij}^* = \langle R_i R_j \rangle$ is the conformation tensor associated with the deformation of polymer microstructures; and $R_i$ is the dimensionless end-to-end vector describing a polymer chain, $\langle \cdots \rangle$ represents the ensemble average. In the FENE-P model, the Peterlin function $f(R) = (L^2 - 2)/(L^2 - R^2)$ ensures the finite extensibility, where $R = \sqrt{\text{trace}(C_{ij}^*)}$ and $L$ are the extension length and the maximum possible extension length of polymer microstructures, respectively. A large $L$ means that the fluid may exhibit more apparent elastic features of polymer solution.

In this paper, the non-Boussinesq effect in thermal convection is not considered.[34] Based on the Boussinesq approximation and FENE-P model for polymer solution, the dimensionless governing equations for single plume flow are expressed as follows:

conservation of mass

$$\frac{\partial u_i^*}{\partial x_i^*} = 0, \tag{1}$$

conservation of momentum

$$\frac{\partial u_i^*}{\partial t^*} + u_j^* \frac{\partial u_i^*}{\partial x_j^*} = -\frac{\partial p^*}{\partial x_i^*} + \frac{\beta}{\sqrt{Ra/Pr}} \frac{\partial}{\partial x_j^*}\left(\frac{\partial u_i^*}{\partial x_j^*}\right) + \frac{1-\beta}{Wi\sqrt{Ra/Pr}} \frac{\partial C_{ij}^*}{\partial x_j^*} + \theta^* \delta_{i2}, \tag{2}$$

conformation transport equation (FENE-P model)

$$\frac{\partial C_{ij}^*}{\partial t^*} + u_j^* \frac{\partial C_{ij}^*}{\partial x_j^*} = C_{ij}^* \frac{\partial u_j^*}{\partial x_j^*} + C_{ij}^* \frac{\partial u_i^*}{\partial x_i^*} - \frac{f(R)C_{ij}^* - \delta_{ij}}{Wi}, \tag{3}$$

and conservation of energy

$$\frac{\partial \theta^*}{\partial t^*} + u_j^* \frac{\partial \theta^*}{\partial x_j^*} = \frac{1}{\sqrt{RaPr}} \frac{\partial}{\partial x_j^*}\left(\frac{\partial \theta^*}{\partial x_j^*}\right), \tag{4}$$

where $\beta = \eta_s/(\eta_s + \eta_p)$ is the ratio of the solvent viscosity to the total viscosity, measuring the polymer concentration by assuming that it only affects the polymer concentration; $\eta_s$ represents the solvent viscosity; and $\eta_p$ represents the viscosity contribution due to polymers. The dimensionless governing parameters: Rayleigh number ($Ra$) and Prandtl number ($Pr$) are defined as $Ra = \alpha g T_h (H/3)^3/\nu\kappa$ and $Pr = \nu/\kappa$, respectively, where $\nu$ and $\kappa$ represent the kinematic viscosity and thermal diffusivity of the working fluid, respectively. The other parameter Weissenberg number $[Wi = \lambda u_c/(H/3)]$ describes the strength of elasticity in polymer solution, where $\lambda$ is the relaxation time of polymer solution. A high $Wi$ means a high history dependence of conformation tensor or strong elastic stress. The elastic stress $\tau_{ij}^*$ is expressed as $\tau_{ij}^* = (1 - \beta)(f(R)C_{ij}^* - \delta_{ij})/Wi$ with $\delta_{ij}$ being the Kronecker symbol.

## C. Kinetic energy budget

For convenience of analyzing energy transfer and contribution, the kinetic energy budget equation in thermal convection with viscoelastic fluid is introduced. According to Eqs. (2) and (3), the balance for the instantaneous kinetic energy can be derived as

$$\frac{dE}{dt} = D + F + V + G, \tag{5}$$

where $E = \frac{1}{2}u_i^* u_i^*$ is the global kinetic energy; $D = \frac{\partial}{\partial x_j^*}\left(pu_i^* - \frac{\beta}{\sqrt{Ra/Pr}}\frac{\partial E_{ij}}{\partial x_j^*} - u_i^*\tau_{ij}^*\right)$ is the kinetic diffusion; $F = \theta^*\delta_{i2}u_i^*$ is the thermal energy input; $V = -\frac{\beta}{\sqrt{Ra/Pr}}\left(\frac{\partial u_i^*}{\partial x_j^*}\frac{\partial u_i^*}{\partial x_j^*}\right)$ is the viscous dissipation of kinetic energy; and $G = -\frac{1-\beta}{Wi\sqrt{Ra/Pr}}\left(C_{ij}^*\frac{\partial u_i^*}{\partial x_j^*}\right)$ represents the energy exchange between flow structures and polymer microstructures due to the stretching and relaxation of polymer chains. The energy exchange term G is assumed as a kind of energy dissipation so that $\eta_{eff}$ can be obtained by

$$-\frac{1-\beta}{Wi\sqrt{Ra/Pr}}\left(C_{ij}^*\frac{\partial u_i^*}{\partial x_j^*}\right) = -\frac{\eta_{eff}}{\eta_s + \eta_p}\frac{1}{\sqrt{Ra/Pr}}\left(\frac{\partial u_i^*}{\partial x_j^*}\frac{\partial u_i^*}{\partial x_j^*}\right), \tag{6}$$

and then the ratio of the effective viscosity to the total viscosity can be written as

$$\frac{\eta_{eff}}{\eta_s + \eta_p} = \beta\frac{G}{V}. \tag{7}$$

Furthermore, the ratio of the effective total viscosity to the original total viscosity is

$$r = \frac{\eta_{eff}}{\eta_s + \eta_p} + \beta = \beta\left(1 + \frac{G}{V}\right), \tag{8}$$

where V is always negative due to energy dissipation. $G < 0$ indicates that energy is absorbed from flow structures into polymer microstructures, vice versa. As long as $r < 1$, it indicates that heat transport is enhanced due to the addition of polymers.

### D. Numerical schemes and grid independence

In our previous study,[35] a procedure embedded with a log-conformation reformulation (LCR) module was established for studying turbulent RBC with polymers. It is noted that the polymer solution in the present study is still considered as conventional continuous medium in macroscopic scale.[36] Here, a similar one is adopted and the detailed parameters are set according to the present research topic. The time-marching uses a mixed Crank-Nicholson with the Pressure-Implicit with Splitting of Operators (PISO) algorithm to solve the coupling of velocity and pressure field. For the convective term, the MINMOD scheme[37] is adopted for the conformation transport equation in order to avoid the deviation caused by large gradient; and the QUICK scheme[38] is selected for the momentum equation and energy equation.

Grid dependence tests are carried out by varying a grid number in vertical and horizontal directions. It shows that the horizontal one has more apparent effect on flow and heat transport due to the large gradient of the conformation tensor. Test results of grid independence in the horizontal direction are shown in Fig. 2. Here, $n$ represents the grid number in the heat source so the grid number in the horizontal direction is $100n$ and the grid resolution is $0.01/n$. As $n$ increases, the Nusselt number ($Nu$) increases and saturates finally. Wherein, $Nu$ is defined as the dimensionless mean temperature gradient averaged over the heat source boundary at steady state

$$Nu = -\int_{-0.005}^{0.005} \left.\frac{\partial \theta^*}{\partial y}\right|_{y=0} dx. \qquad (9)$$

The difference of $Nu$ is smaller than 0.25% when $n$ reaches 11. Accordingly, a uniform finer $1100 \times 750$ mesh coupled with time step $5 \times 10^{-3}$ is used for all runs.

According to the experience in experiments, $Pr$ and $\beta$ for polymer solution are in the range 7–100 and 0.4–1, respectively. In order to generate the steady single plume, the simulations are performed using the FENE-P model to represent
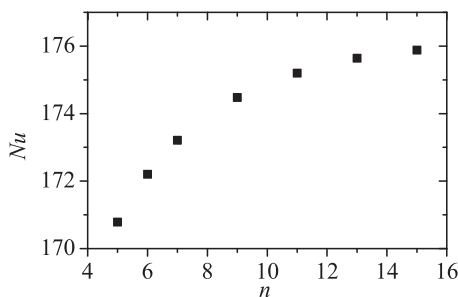
polymers and some parameters are set as $Pr = 50$ and $\beta = 0.6$. To evaluate the elastic effect on the plume dynamic, $Wi$ and $L$ ranges from 1 to 10 and from 10 to 40, respectively. Additionally, the Newtonian fluid case is simulated by setting $\beta = 1$.

## III. RESULTS AND DISCUSSION

### A. Effect of *Wi* on flow and heat transport

Since a single plume has been extensively investigated, the conclusion already known will not be repeated but the development of the plume is described in this section. As an example, Fig. 3 plots the time evolution of $Nu$ at different $Wi$ cases with the same $L = 10$, where $Wi = 0$ represents the Newtonian fluid case. The dynamic process of single plume flow can be classified into three stages according to the physical phenomena: start-up stage, break-through stage, and stable-ascend stage. In the start-up stage, heat is mainly transported by conduction into fluid and the temperature gradient at the boundary of the heat source drops sharply. The fluid starts to rise due to buoyance force, but the plume is still semi-circle cell as shown in Fig. 4(a). In the break-through stage, the amount of heat transported by convection increases a lot and the heat transport rapidly reaches the peak and returns to a steady state, which is so-called overshoot (see Ref. 39). During this stage, hot fluid breaks through from the semicircle cell and the cap of the plume is taking shape, as shown in Fig. 4(b). After the overshoot passes, the heat transport reduces gradually to a constant value. As shown in Fig. 4(c), a standard single plume forms in the stable-ascend stage and it is characterized by a large "cap" at the top of a thinner "stem" with two "ears." In fact, the plume still grows wider continually due to the diffusion effect from Eq. (4) as it rises. In this study, the plume can ascend stably in the third stage mainly due to high $Pr$, otherwise the stem flaps periodically.[40]

As shown in Fig. 3, the heat transport in the stable-ascend stage decreases with the increasing $Wi$, and the durations for such three stages become longer due to the increase of $Wi$. It
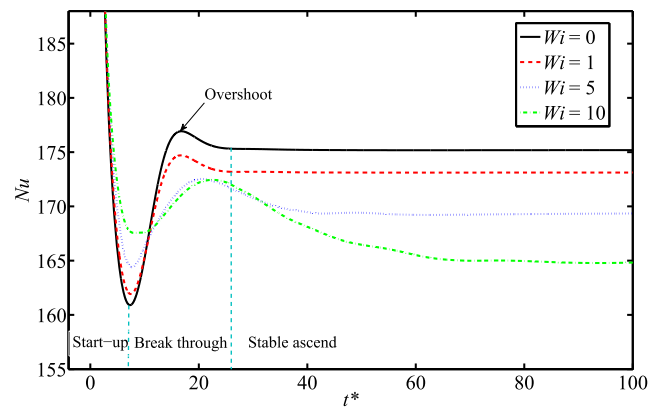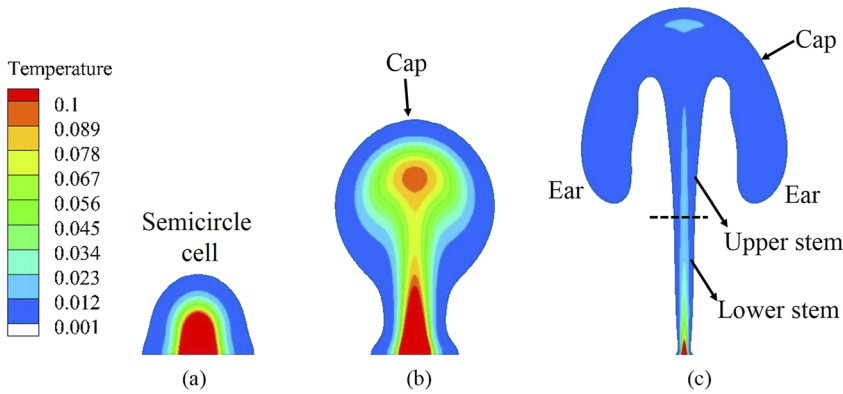
**FIG. 2**. $Nu$ as a function of the grid number in the heat source.

**FIG. 3**. Time evolution of $Nu$ at different $Wi$ with $L = 10$. $Wi = 0$ represents the Newtonian fluid case. Three stages are marked by vertical dashed lines.

**FIG. 4**. The evolution of the plume in the Newtonian fluid case at three stages (a) start-up stage $t^* = 8$; (b) break-through stage $t^* = 20$; and (c) stable-ascend stage $t^* = 100$.

costs time to release the energy absorbed from flow structures due to the extension and relaxation of polymers. Therefore, the developing time for three stages is longer as $Wi$ increases. In the break-through stage, the variation magnitude of $Nu$ also decreases with $Wi$ and the overshoot phenomenon is suppressed slightly. In sum, the elasticity inhibits single plume flow in polymer solution cases from either the duration or the amplitude of oscillation.

Figure 5 plots the time series of vertical velocities for different $Wi$ cases in a monitor point close to the heat source, P (0, 0.1). It can be seen that the vertical velocity $u_y^*$ becomes constant at last which is consistent with the scaling argument in Ref. 17. It is worth mentioning that $u_y^*$ in the start-up stage is larger with the increasing $Wi$ and there exists an intersection after which the variation turns and heat transport in cases with higher $Wi$ is smaller. In fact, polymers cannot response rapidly to the flow variation due to the stretching and relaxation of polymers when heat is suddenly transported into the domain. It results in that the viscous dissipation term V dominates in Eq. (5), which is smaller than that in the Newtonian fluid case. Therefore, the plume in polymer solution cases ascends quickly in a short time due to lower energy dissipation at the start-up stage. Similar results in the start-up stage of Poiseuille flow indicate that the maximum velocity developed in the first stage is larger as elasticity increases.[41] Therefore, the starting of single plume flow can be understood as suddenly imposing a pressure gradient at the inlet in pipe flows, although the buoyancy force is not uniform as the body force.
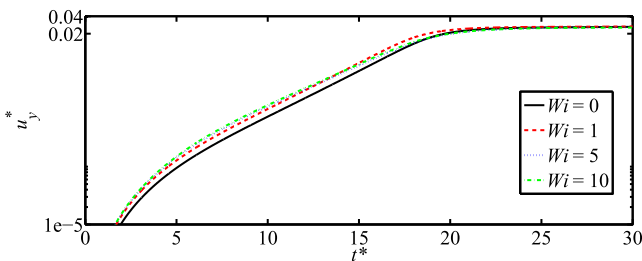
In single plume flow, the stem is the most important structure due to its role of the heat carrier. In the interior of the stem, the horizontal velocity is so small that it can be neglected as being compared to the vertical one. Figure 6 plots the temperature and vertical velocity $u_y^*$ distribution over the $y$ axis at the final stage for various $Wi$ cases with L = 10. As shown in Fig. 6(b), the vertical velocities exist a peak value $(u_y^*)_{max}$ along the stem. In the lower stem ($y \leq y[(u_y^*)_{max}]$), vertical velocities and temperatures are close along the stem. When the fluid arrives at the upper stem ($y \geq y[(u_y^*)_{max}]$), it is interesting that $u_y^*$ in all polymer solution cases are larger than that in the Newtonian fluid case, whereas $u_y^*$ decreases with the increasing of $Wi$. Meanwhile, the temperature decreases slowly along the stem and then reaches a small peak followed by a sharp drop to zero when the fluid arrives at the plume boundary. The plume height is defined as the farthest position away from the heat source at which temperature reduces to zero. It is observed that the plume height in the Newtonian fluid case is the lowest due to small ascend velocity, as shown in Fig. 6(a). In sum, polymers promote the ascend of the plume, but the promotion gets weaker with the increasing of $Wi$.

To further investigate the elastic effect on the plume flow, it is necessary to plot the contours of the whole field apart from the distribution along one line. Figure 7 shows the contours of vertical velocity $u_y^*$ and temperature at $t^* = 20$ for the Newtonian fluid case and $Wi = 10$ and $L = 10$ case. When the break-through stage starts, in the lower stem, the vertical velocity in downstream is larger than that in upstream so that polymers are stretched due to velocity difference. Part of energy input from the heat source is stored as elastic energy, which in turn suppresses the acceleration of the vertical velocity. Therefore, in comparison with the almond-like pattern in the Newtonian fluid case, the center of pattern in the polymer solution case has a sunken region which forms a tooth-like pattern, as shown in Fig. 7(b). This pattern also keeps well at the stable ascend stage.

For the contour of the temperature field in Figs. 7(c) and 7(d), a new high-temperature region appears at the core of the plume head comparing with Fig. 4(a). It departs from the heat source and transports heat to the surrounding fluids by
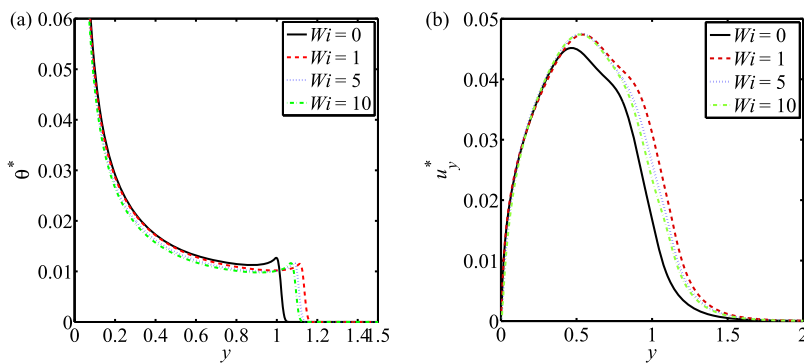


**FIG. 5**. Time series of vertical velocities at monitor P (0, 0.1) for different $Wi$ cases.

**FIG. 6**. Profiles of variables along axis $y$ at $t^* = 100$ for various $Wi$ cases with $L = 10$ (a) temperature $\theta^*$ and (b) vertical velocity $u_y^*$.

convection. A lower-temperature plume head indicates that polymer solution cases have a quicker heat losing rate, implying a stronger local thermal convection.

A more direct understanding of the elastic effect on flow dynamics can be obtained by calculating the energy exchange term G. Figure 8 plots the contour of G and velocity vector field at the final stage for Wi = 10 and L = 10 case. To make it more clear, the regimes of G > 0 and smaller negative G are marked with red and white, respectively. The plume boundary is also marked with $\theta^* = 10^{-5}$ by the blue line.

With the rising of the plume, hot fluid driven by temperature difference separates into two directions at the top
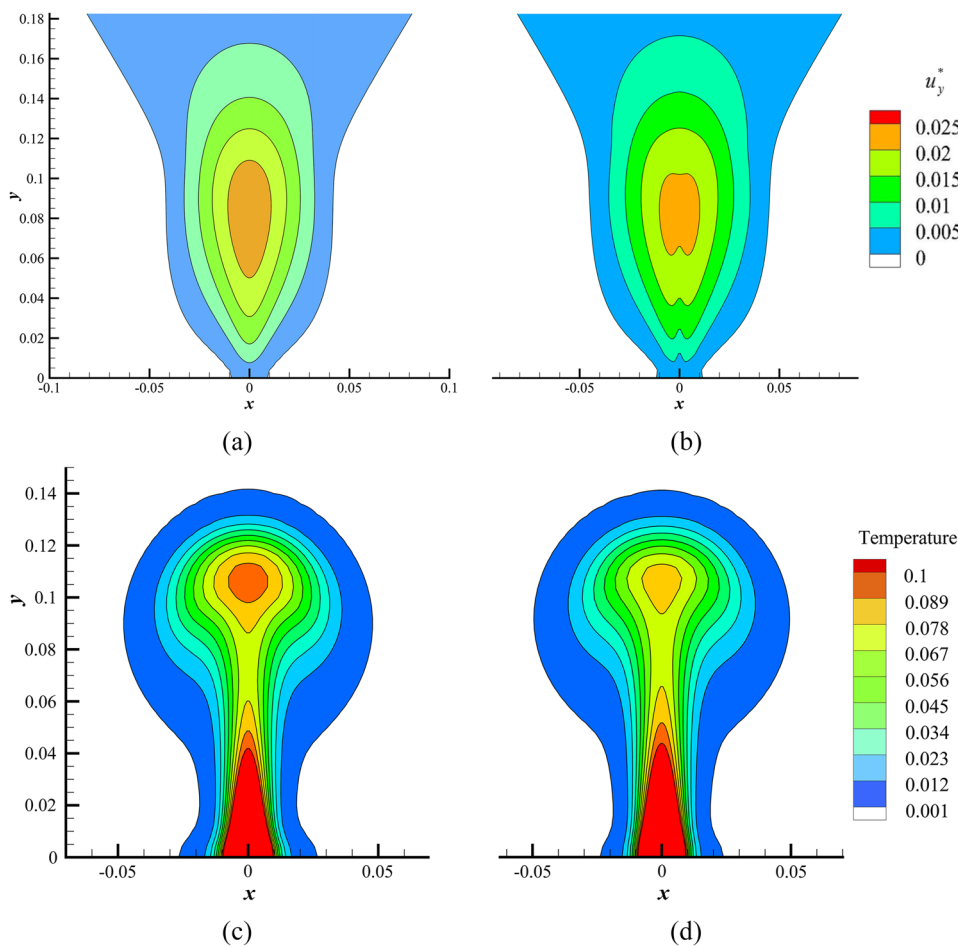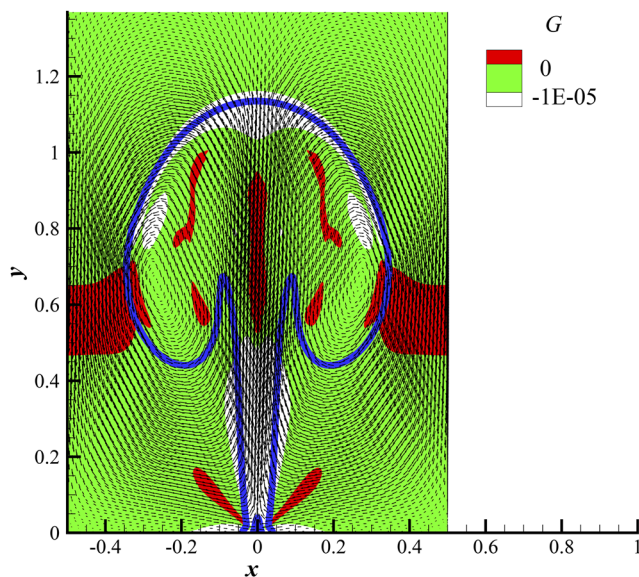


**FIG. 7**. The contours of vertical velocity $u_y^*$ [(a) and (b)] and temperature [(c) and (d)] at $t^* = 20$ for the Newtonian fluid case [(a) and (c)] and $Wi$ = 10 and $L$ = 10 case [(b) and (d)]. The lowest level is overrode by white color.

**FIG. 8**. Contour of $G$ and vector field of velocity at $t^* = 100$ with $Wi = 10$ and $L = 10$ case. The plume boundary is marked with $\theta^* = 10^{-5}$ by the blue line. $G > 0$ indicates that energy is released from polymer microstructures into flow structures, vice versa.
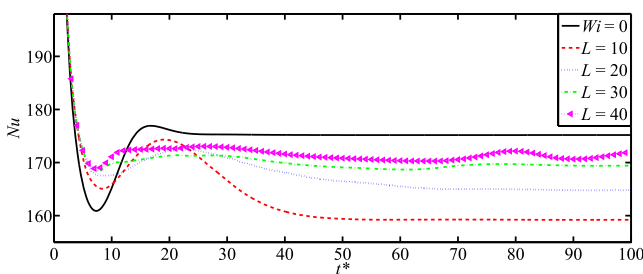


**FIG. 9**. Time evolution of $Nu$ at different $L$ cases with $Wi = 10$.

region of the plume cap. Meanwhile, cold fluid is entrained by the plume and then mixed with hot one, which thereby form large vortexes at the plume ears, as shown in Fig. 8. It is observed that the positive $G$ mainly occurs in the upper stem and the inner side of ears, whereas the negative one occupies most of the flow field. In fact, positive $G$ also occurs at the outer region, but its value is small due to low velocity gradient, namely, that the relaxation is insufficient. It can be understood that positive $G$ tends to occur at the position where the velocity is decelerated. As mentioned above, the acceleration in the lower stem is suppressed by elastic stress. It is verified from the white region in the lower stem where polymer microstructures absorb much energy from flow structures due to the stretching of polymers. Then, attention is paid to the cap region, and white contour indicates that polymers here can also be stretched greatly. It can be explained that the buoyancy force is not enough to overcome the resistance when the fluid ascends to the top of the plume. Therefore, the fluid flow has to be separated into two directions which of course results in the stretching of polymers. In addition, the white region near the heat source also provides a direct explanation about the HTR induced by polymers within the boundary layer.[42]

## B. Effect of $L$ on flow and heat transport

To solely evaluate the effect of $L$ on flow and heat transport, $Wi$ is fixed in this section. As an example, the time evolution of $Nu$ at different $L$ cases with $Wi = 10$ is shown in Fig. 9. It is observed that the evolution process can still be classified into three stages, and the durations for each stage become longer. In addition, the overshoot phenomenon becomes not obvious and the peak value in the break-through stage decreases as $L$ increases. Particularly, the flow in the case with $L = 40$ starts to oscillate in the stable-ascend stage. The main effect of $L$ is HTR, whereas the amount reduces with the increasing $L$ within the range studied in this paper.

The profiles of temperature and velocity along $x = 0$ at $t^* = 100$ are plotted for various $L$ cases in Fig. 10. The characteristics of these two profiles and the comparison with the Newtonian fluid case are described in Fig. 6. Considering polymer solution cases, the vertical velocity decreases and the temperature increases with the increasing $L$. A higher vertical velocity results in lower temperature in the stem and higher plume height, which gets mutual verification.
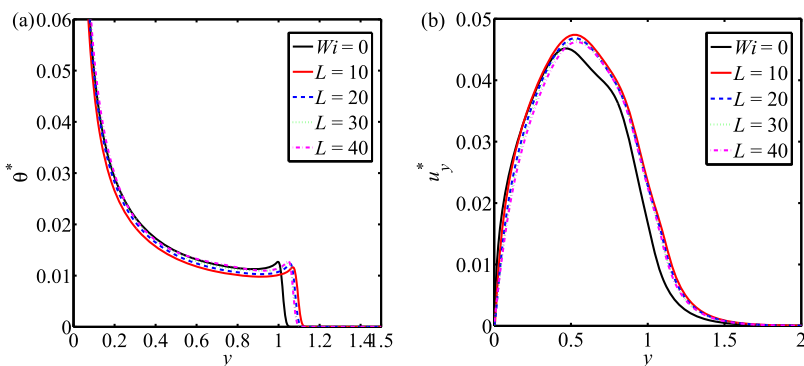


**FIG. 10**. Profiles of variables along axis $y$ at $t^* = 100$ for various $L$ cases with $Wi = 10$ (a) temperature $\theta^*$ and (b) vertical velocity $u_y^*$.
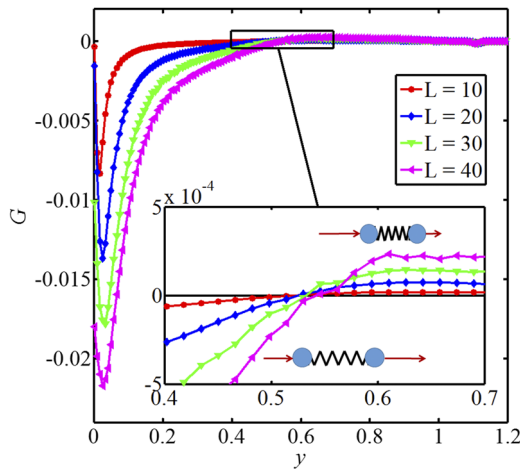
**FIG. 11**. Profiles of $G$ over the vertical line $x = 0$ at $t^* = 100$ for various $L$ cases with $Wi = 10$. The inset is the enlarged plot for the transition of sign of $G$ and schematically shows the mechanism of energy exchange. $G < 0$ indicates that energy is absorbed from flow structures into polymer microstructures, vice versa.

The contour of energy exchange term $G$ for polymer solution cases is discussed in Fig. 8. To explain the effect of $L$ on flow and heat transport, Fig. 11 plots the profiles of $G$ over $x = 0$ at $t^* = 100$ for various $L$ cases with $Wi = 10$. It can be seen that $G$ decreases rapidly followed by a gradual increase along the lower stem and it becomes positive in the upper stem although the value is relatively small. The increase of $G$ with the increasing $L$ in the upper stem results in stronger thermal convection in the cap region, which in turn enhances heat transport. It is noted that the valley position of $G$ goes up along the $y$ direction due to the increase of extension length $L$.

As shown in Figs. 10 and 11, the transition position of absorbing and releasing energy locates at the half length of the stem. The horizontal line $y = 0.8$ crosses the upper stem, over which the profiles of $G$ for various $L$ cases are shown in Fig. 12(a). It is observed that only small regions near the stem has positive $G$ and the remaining regions absorb energy from

flow structures. It is worth mentioning that the position with the highest energy absorption occurs at the plume boundary. The boundary moves towards the stem with the increasing $L$, which indicates the plume with small $L$ is wider. Figure 12(b) plots the profile of the ratio between effective total viscosity and original total viscosity. It shows that the ratios in the region $x \leq 6d$ are smaller than 1, implying that heat transport is enhanced and HTE increases with the increasing $L$ in this region.

## C. Discussion

The dynamic process of single plume flow in the polymer solution case has been investigated by varying the governing parameters $Wi$ and $L$, respectively. To make it clear, we would like to explain the process simply from the view of polymer chains travelling in the plume. As schematically shown in Fig. 13, polymer chains are represented by two dumbbells connected by a finitely extensible spring. According to the distribution of the vertical velocity, the stem is divided into two parts. As polymer chains travel in the lower stem, as shown in Fig. 13(a), the slower dumbbell cannot follow up the quicker one in time so that the spring will be stretched. Therefore, the energy is absorbed from flow structures and stored in polymer chains in the lower stem. Afterwards, polymer chains continue to ascend with fluid. When they arrive at the upper stem, the velocity of the lower dumbbell exceeds that of the upper one, as shown in Fig. 13(b). The spring relaxes and releases energy into flow structures. Figure 13(c) illustrates that polymer chains are stretched due to the flow separation at the top region of the cap.

For the effect on heat transport, a dependence relation with the governing parameters is expected. Figure 14 plots $Nu$ as a function of $Wi$ in the stable-ascend stage for different $L$ cases. It is seen that the parameter $L$ has no effect on heat transport for $Wi = 1$, whereas $Nu$ increases with the increase of $L$ for $Wi = 5$ and 10. Specifically, the HTE phenomenon occurs in $Wi = 5$ and $L = 40$ case. To make it more universal, the two effects induced by $Wi$ and $L$ are coupled. Figure 15 shows the dependence of the ratio of $Nu$ on the governing parameter $L^2/Wi$ in polymer solution cases. By applying a power-law fitting, the formula of the ratio $Nu/Nu_{New}$ can be written as (see
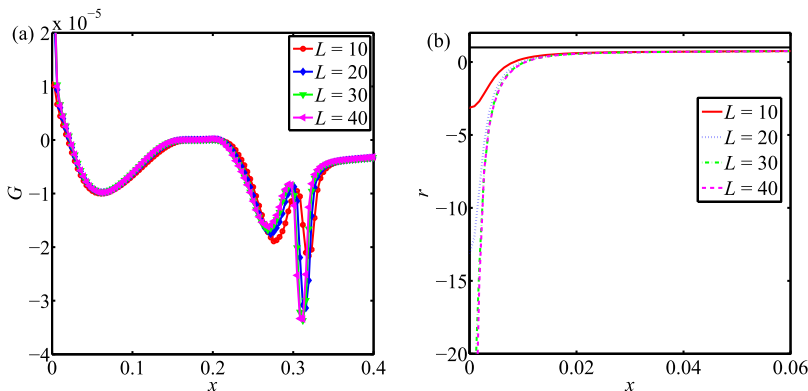


**FIG. 12**. Profiles of (a) $G$ and (b) the ratio $r$ between total effective viscosity and original total viscosity over the horizontal line $y = 0.8$ at $t^* = 100$ for various $L$ cases with $Wi = 10$. $G < 0$ indicates that energy is absorbed from flow structures into polymer microstructures, vice versa. The solid black line $r = 1$ represents the Newtonian fluid case.
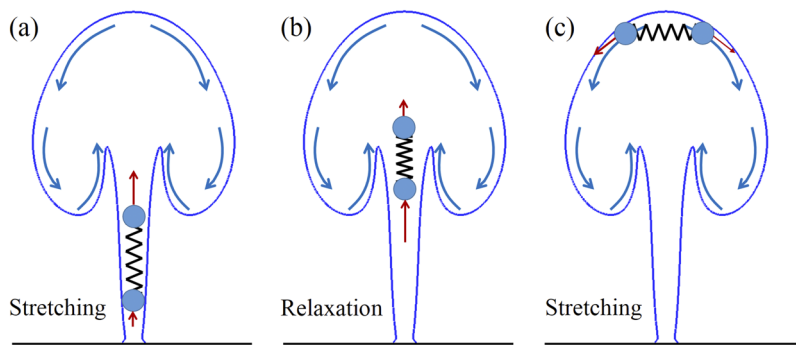
**FIG. 13**. Schematic of the dynamic process of polymer microstructures as they travel in the plume. (a) Stretching in the lower stem; (b) relaxation in the upper stem; and (c) stretching in the boundary of the cap.
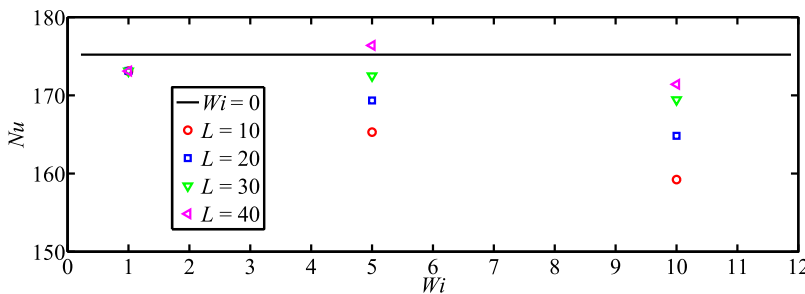


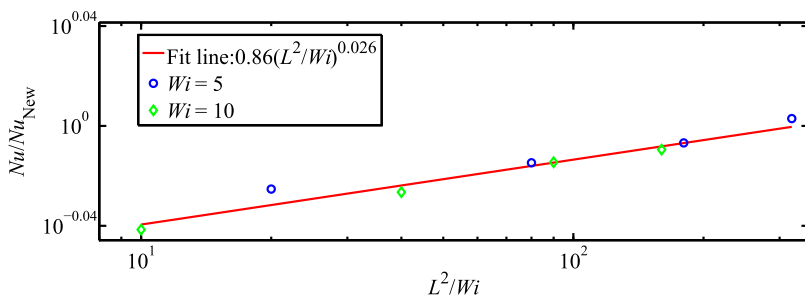**FIG. 14**. $Nu$ as a function of $Wi$ in the stable-stage for different $L$ cases.



**FIG. 15**. Dependence of $Nu/Nu_{New}$ on the governing parameters $L^2/Wi$ in polymer solution cases. The axes are in logarithmic scale.

also Fig. 15)

$$Nu/Nu_{New} = 0.86(L^2/Wi)^{0.026}, \qquad (10)$$

wherein $Nu$ for $Wi = 1$ is not adopted due to the ignorable effect of $L$. It is obvious that this formula is unreasonable when $L$ approaches infinite or $Wi$ reduces to be infinitely small. In fact, the Peterlin function $f(R)$ should be considered instead of $L$ as deducing a formula about the ratio $Nu/Nu_{New}$. However, $f(R)$ is related to not only $L$ but also the real extension length $R$ which is not a constant in flow. Therefore, it remains for more studies to give new insight into single plume flow at some extreme parameters. The formula deduced in the present study is only applicable for moderate $Wi$ and small $L$.

## IV. CONCLUSIONS

In order to obtain more intuitive cognition on thermal plumes in polymer solution, we simulated the single plume flow generated from a point heat source and adopted an FENE-P model to represent polymers. We investigated the effects of elasticity and maximum extensional length $L$ on flow and heat transport ability, respectively. We also figured out the dynamic process of energy exchange between polymer microstructures and flow structures in the plume.

Based on the profile of vertical velocity and temperature along the $y$ axis, it is seen that the plume in polymer solution is speeded up and widens in comparison with that in the Newtonian fluid case. The start-up plume flow can be approximately interpreted as suddenly imposing a constant pressure gradient at the inlet in pipe flows. In this stage, the ascend velocity increases with the increasing $Wi$ and $L$. In the stable-ascend stage, the stem is divided into two parts. The vertical velocity decreases with the increasing $Wi$ and $L$ in the upper stem. It can be understood that the energy absorbed from flow structures takes more time and distances to be released due to larger $Wi$ or $L$.

The inhibition effect of $Wi$ and promotion effect of $L$ on heat transport in a single plume can give direct insight into

the observation about plumes in turbulent thermal convection experiments.[9,11–14] For the maximum extension length $L$, the HTE effect appears for lower values of $L \leq 50$, and $Nu$ increases when $L$ is smaller than 20 in turbulent thermal convection.[13] The difference may result from the choice of higher $Ra$ and $Pr$ so that the range of $L$ investigated here is still smaller than the turning point. As for the dynamic process of energy exchange, it is determined by the flow field. As polymer chains travel in the plume, they absorb energy in the lower stem and release energy in the upper stem. Continually, they absorb energy in the cap region and release energy in the inner boundary of plume ears. It remains for future studies to explore the relation between single plume and fully turbulent thermal convection.

Although the former feature is specific for the present configuration, we think that our findings can be more general than the specific setup studied. Moreover, the single plume can also be realized in laboratory experiments and therefore our results based on numerical simulations of primitive equations are the good starting point for experimental investigation on the effect of polymers on the turbulent buoyancy-driven system.

## REFERENCES

[1] G. Ahlers, S. Grossmann, and D. Lohse, "Heat transfer and large scale dynamics in turbulent Rayleigh-Bénard convection," Rev. Mod. Phys. **81**, 503 (2009).

[2] D. Lohse and K.-Q. Xia, "Small-scale properties of turbulent Rayleigh-Bénard convection," Annu. Rev. Fluid Mech. **42**, 335 (2010).

[3] H.-D. Xi, S. Lam, and K.-Q. Xia, "From laminar plumes to organized flows: The onset of large-scale circulation in turbulent thermal convection," J. Fluid Mech. **503**, 47 (2004).

[4] K.-Q. Xia, C. Sun, and S.-Q. Zhou, "Particle image velocimetry measurement of the velocity field in turbulent thermal convection," Phys. Rev. E **68**(6), 066303 (2003).

[5] X.-D. Shang, X.-L. Qiu, P. Tong, and K.-Q. Xia, "Measured local heat transport in turbulent Rayleigh-Bénard convection," Phys. Rev. Lett. **90**, 074501 (2003).

[6] X.-D. Shang, X.-L. Qiu, P. Tong, and K.-Q. Xia, "Measurements of the local convective heat flux in turbulent Rayleigh-Bénard convection," Phys. Rev. E **70**, 026308 (2004).

[7] Y. Dubief, "Heat transfer enhancement and reduction by polymer additives in turbulent Rayleigh-Benard convection," e-print arXiv:1009.0493v1 [physics.flu-dyn] (2010).

[8] R. B. Bird, O. Hassager, R. C. Armstrong, and C. F. Curtis, *Dynamics of Polymeric Liquids* (Wiley-Interscience, New York, 1987).

[9] G. Boffetta, A. Mazzino, and S. Musacchio, "Effects of polymer additives on Rayleigh-Taylor turbulence," Phys. Rev. E **83**, 056318 (2011).

[10] G. Ahlers and A. Nikolaenko, "Effect of a polymer additive on heat transport in turbulent Rayleigh-Bénard convection," Phys. Rev. Lett. **104**, 034503 (2010).

[11] P. Wei, R. Ni, and K.-Q. Xia, "Enhanced and reduced heat transport in turbulent thermal convection with polymer additives," Phys. Rev. E **86**, 016325 (2012).

[12] T.-Z. Wei, W.-H. Cai, C.-Y. Huang, H.-N. Zhang, W.-T. Su, and F.-C. Li, "The effect of surfactant solutions on flow structures in turbulent Rayleigh-Bénard convection," Therm. Sci. **22**, 507–515 (2018).

[13] W.-H. Cai, T.-Z. Wei, X.-J. Tang, Y. Liu, B. Li, and F.-C. Li, "The polymer effect on turbulent Rayleigh-Bénard convection based on PIV experiments," Exp. Therm. Fluid Sci. **103**, 214 (2019).

[14] Y.-C. Xie, S. D. Huang, D. Funfschilling, X.-M. Li, R. Ni, and K.-Q. Xia, "Effects of polymer additives in the bulk of turbulent thermal convection," J. Fluid Mech. **784**, R3 (2015).

[15] M. Lappa and H. Ferialdi, "Multiple solutions, oscillons, and strange attractors in thermoviscoelastic Marangoni convection," Phys. Fluids **30**, 104104 (2018).

[16] T. Ukai, H. Zare-Behtash, and K. Kontis, "Suspended liquid particle disturbance on laser-induced blast wave and low density distribution," Phys. Fluids **29**, 126104 (2017).

[17] G. K. Batchelor, "Heat convection and buoyancy effects in fluids," Q. J. R. Meteorol. Soc. **80**, 339–358 (1954).

[18] T. Fuji, "Theory of the steady laminar natural convection above a horizontal line heat source and a point heat source," Int. J. Heat Mass Transfer **6**, 597–606 (1963).

[19] R. S. Brand and F. J. Lahey, "The heated laminar vertical jet," J. Fluid Mech. **29**(2), 305–315 (1967).

[20] B. Gebhart, L. Pera, and A. Schorr, "Steady laminar natural convection plumes above a horizontal line heat source," Int. J. Heat Mass Transfer **13**, 161–171 (1970).

[21] M. G. Worster, "The axisymmetric laminar plume: Asymptotic solution for large Prandtl number," Stud. Appl. Math. **75**(2), 139–152 (1986).

[22] D. J. Shlien, "Some laminar thermal and plume experiments," Phys. Fluids **19**(8), 1089–1098 (1976).

[23] E. Moses, G. Zocchi, and A. Libchaberii, "An experimental study of laminar plumes," J. Fluid Mech. **251**, 581–601 (1993).

[24] E. Kaminski and C. Jaupart, "Laminar starting plumes in high-Prandtl-number fluids," J. Fluid Mech. **478**, 287–298 (2003).

[25] A. Davaille, L. Angela, T. Floriane, K. Ichiro, and V. Judith, "Anatomy of a laminar starting thermal plume at high Prandtl number," Exp. Fluids **50**(2), 285–300 (2011).

[26] M. C. Rogers and S. W. Morris, "Natural versus forced convection in laminar starting plumes," Phys. Fluids **21**, 083601 (2009).

[27] R. J. Whittaker and R. L. John, "Steady axisymmetric creeping plumes above a planar boundary. Part 1. A point source," J. Fluid Mech. **567**, 361–378 (2006).

[28] S. Paillat and E. Kaminski, "Entrainment in plane turbulent pure plumes," J. Fluid Mech. **755**, R2 (2014).

[29] B. Vajipeyajula, T. Khambampati, and R. A. Handler, "Dynamics of a single buoyant plume in a FENE-P fluid," Phys. Fluids **29**, 091701 (2017).

[30] G. S. Gunasegarane and B. A. Puthenveettil, "Dynamics of line plumes on horizontal surfaces in turbulent convection," J. Fluid Mech. **749**, 37–78 (2014).

[31] R. Sureshkumar and A. N. Beris, "Effect of artificial stress diffusivity on the stability of numerical calculations and the flow dynamics of time-dependent viscoelastic flows," J. Non-Newtonian Fluid Mech. **60**, 53 (1995).

[32] C. D. Dimitropoulos, R. Sureshkumar, and A. N. Beris, "Direct numerical simulation of viscoelastic turbulent channel flow exhibiting drag reduction: Effect of the variation of rheological parameters," J. Non-Newtonian Fluid Mech. **79**, 433 (1998).

[33] E. De Angelis, C. M. Casciola, and R. Piva, "DNS of wall turbulence: Dilute polymers and self-sustaining mechanisms," Comput. Fluids **31**, 495 (2002).

[34] Y. Zhang and Y. Cao, "A numerical study on the non-Boussinesq effect in the natural convection in horizontal annulus," Phys. Fluids **30**, 040902 (2018).

[35] J.-P. Cheng, H.-N. Zhang, W.-H. Cai, S. N. Li, and F.-C. Li, "Effect of polymer additives on heat transport and large-scale circulation

in turbulent Rayleigh-Bénard convection," Phys. Rev. E **96**(1), 013111 (2017).

[36] T. Ye, D. Pan, C. Huang, and M. Liu, "Smoothed particle hydrodynamics (SPH) for complex fluid flows: Recent developments in methodology and applications," Phys. Fluids **31**, 011301 (2019).

[37] B. Yu and Y. Kawaguchi, "Direct numerical simulation of viscoelastic drag-reducing flow: A faithful finite difference method," J. Non-Newtonian Fluid Mech. **116**, 431 (2004).

[38] B. P. Leonard, "A stable and accurate convective modelling procedure based on quadratic upstream interpolation," Comput. Methods Appl. Mech. Eng. **19**, 59–98 (1979).

[39] F. Xu and J. C. Patterson, "Temperature oscillations in a differentially heated cavity with and without a fin on the sidewall," Int. Commun. Heat Mass Transfer **37**(4), 350–359 (2010).

[40] M.-M. Qiao, F. Xu, and C. S. Suvash, "Scaling analysis and numerical simulation of natural convection from a duct," Numer. Heat Transfer, Part A **72**(5), 355–371 (2017).

[41] A. I. P. Miranda and P. J. Oliveira, "Start-up times in viscoelastic channel and pipe flows," Korea-Aust. Rheol. J. **22**(1), 65–73 (2010).

[42] R. Benzi, E. S. C. Ching, and V. W. S. Chu, "Heat transport by laminar boundary layer flow with polymers," J. Fluid Mech. **696**, 330–344 (2012).